Organic–Inorganic Hybrid Materials | Hot Paper

DOI: 10.1002/ange.201311136

Engineering Multifunctional Capsules through the Assembly of Metal–Phenolic Networks**

*Junling Guo, Yuan Ping, Hirotaka Ejima, Karen Alt, Mirko Meissner, Joseph J. Richardson, Yan Yan, Karlheinz Peter, Dominik von Elverfeldt, Christoph E. Hagemeyer, and Frank Caruso**

Abstract: *Metal–organic coordination materials are of widespread interest because of the coupled benefits of inorganic and organic building blocks. These materials can be assembled into hollow capsules with a range of properties, which include selective permeability, enhanced mechanical/thermal stability, and stimuli-responsiveness. Previous studies have primarily focused on the assembly aspects of metal-coordination capsules; however, the engineering of metal-specific functionality for capsule design has not been explored. A library of functional metal–phenolic network (MPN) capsules prepared from a phenolic ligand (tannic acid) and a range of metals is reported. The properties of the MPN capsules are determined by the coordinated metals, allowing for control over film thickness, disassembly characteristics, and fluorescence behavior. Furthermore, the functional properties of the MPN capsules were tailored for drug delivery, positron emission tomography (PET), magnetic resonance imaging (MRI), and catalysis. The ability to incorporate multiple metals into MPN capsules demonstrates that a diverse range of functional materials can be generated.*

Naturally occurring building blocks that can assemble into functional materials have long been a source for scientific inspiration.[1] A salient feature of natural materials is the exploitation of organic and inorganic building blocks to prepare hybrid materials with synergistic properties to meet complex biological requirements.[1a,d] For example, by using mild conditions to generate highly functional macroscopic inorganic–organic hybrids, crustaceans produce armoured carapaces,[1d] mollusks build ornate shells,[2] and vertebrates grow lightweight bones.[1d] Specifically, the coordination of organic ligands with specific metal species plays a critical role in a range of biological functions,[3] such as photosynthesis (through Mg^{II}-porphyrin),[4] oxygen transportation (through Cu^{II}-heme)[5] and adhesion (through Fe^{III}-phenolics).[6] Inspired by these natural examples, metal–organic coordination materials have attracted considerable interest in chemistry and materials science.[7]

The assembly of metal–organic coordination materials into hollow capsules has recently attracted interest because of their desirable properties,[8] such as selective permeability,[9] high mechanical[10] and thermal[11] stability, and pH-responsive disassembly.[10b] Several assembly techniques, including liquid–liquid interfacial growth,[9a] spray-drying,[9b] and sacrificial template-mediated formation,[10–12] have been used to fabricate capsules based on metal-coordination interactions. However, these previous studies have not focused on the specific incorporation of a range of metals into the capsule shells, nor have the incorporated metals specifically been used to impart functionality into the capsules. The ability to incorporate diverse metals into metal–organic coordination capsules provides new opportunities for engineering multifunctional systems for various applications.

Here, we demonstrate that a single organic ligand can coordinate with a variety of metals, and thereby provide a broad library of functional metal–phenolic networks (MPNs). Because of the diverse chelation ability of phenolic materials,[13] tannic acid (TA; see Figure S1 in the Supporting Information), a ubiquitous natural polyphenol, is coordinated to 18 different metal ions (M), including aluminium (Al), vanadium (V), chromium (Cr), manganese (Mn), iron (Fe), cobalt (Co), nickel (Ni), copper (Cu), zinc (Zn), zirconium

[*] J. Guo, Dr. Y. Ping, Dr. H. Ejima, J. J. Richardson, Dr. Y. Yan, Prof. F. Caruso
Department of Chemical and Biomolecular Engineering
The University of Melbourne, Parkville
Victoria 3010 (Australia)
E-mail: fcaruso@unimelb.edu.au
Dr. K. Alt, Prof. K. Peter, Assoc. Prof. C. E. Hagemeyer
Atherothrombosis and Vascular Biology/Vascular Biotechnology
Baker IDI Heart and Diabetes Institute
Melbourne, Victoria 3010 (Australia)
M. Meissner, Prof. D. von Elverfeldt
Department of Radiology, Medical Physics
University Medical Center Freiburg
Breisacher Str. 60a, Freiburg (Germany)

[**] The authors acknowledge support of this research by the Australian Research Council under the Australian Laureate Fellowship FL120100030 (F.C.), Discovery Project DP0877360 (F.C.), Discovery Early Career Researcher Award DE130100488 (Y.Y.), and Future Fellowship FT0992210 (K.P.) schemes. This work was supported by a project grant from the National Health and Medical Research Council (grant number 1029249; K.P. and C.E.H.). K.A. is supported by the German Research Foundation (grant number Al 1521/1-1). C.E.H. is supported by a National Heart Foundation Career Development Fellowship (grant number CR 11M 6066). The work was also supported in part by the Victorian Government's Operational Infrastructure Support Program, Monash Biomedical Imaging and Victoria's Science Agenda Strategic Project Fund. We acknowledge the Centre for PET at the Austin (Melbourne, Australia) for supply of the ^{64}Cu. We thank X. Wang (Sichuan University) for assistance with the catalytic experiments, X. Duan (The University of Melbourne) for assistance with XPS analysis, Dr. K. Liang (The University of Melbourne) for assistance with deconvolution microscopy, and Dr. Ming Hu, Dr. Jiwei Cui, Yi Ju, and Tomoya Suma (The University of Melbourne) for helpful discussions.

Supporting information for this article is available on the WWW under http://dx.doi.org/10.1002/anie.201311136.

(Zr), molybdenum (Mo), ruthenium (Ru), rhodium (Rh), cadmium (Cd), cerium (Ce), europium (Eu), gadolinium (Gd), and terbium (Tb), to generate robust MPN films capable of forming hollow structured capsules (Figure 1). Given the facile preparation process, and the capacity to incorporate single and multiple metals, MPN capsules are a promising class of multifunctional materials. These MPN capsules are herein characterized and used for diverse applications, including drug delivery, biomedical imaging, and catalysis.

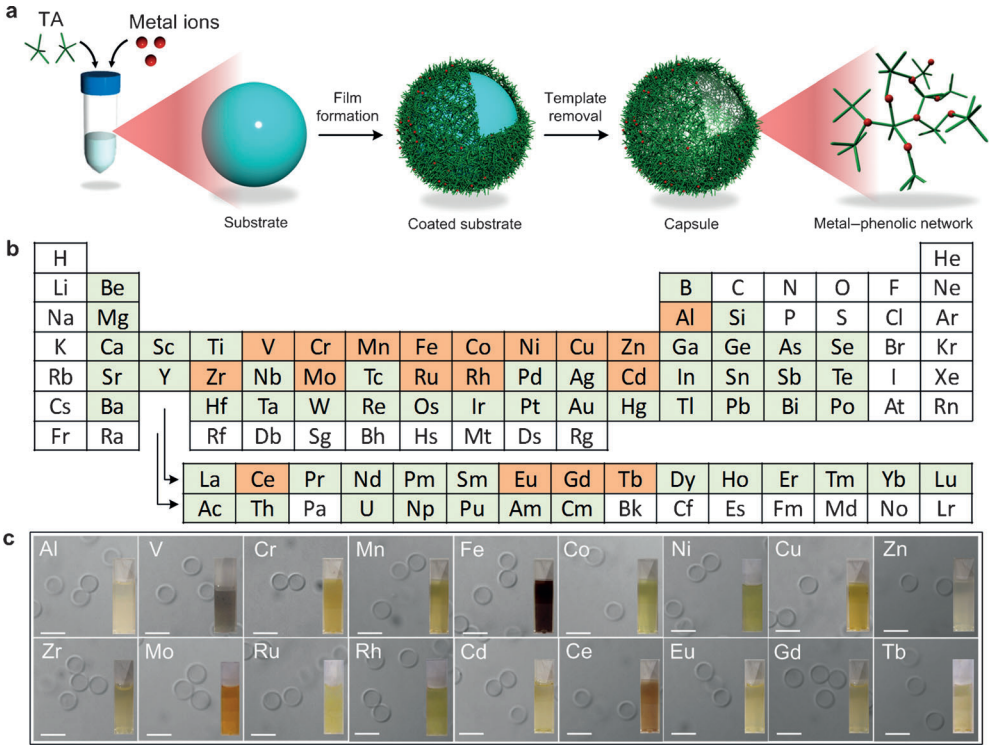

Figure 1. Assembly of MPN capsules from various metals. a) Assembly of TA and metal ions to form a MPN film on a particulate template, followed by the subsequent formation of a MPN capsule. b) Periodic table: metals highlighted in orange are used to form MPN capsules in this study. Metals highlighted in green show other metals that may be used for MPN capsule preparation based on previous studies on metal-coordination with phenolics in bulk solution. c) DIC images of MPN capsules prepared from different metals. Scale bars are 5 μm. Inset images are photographs of MPN capsule suspensions.

MPN films were formed simply by mixing TA and metal solutions in the presence of a substrate (Figure 1a). When using particulate templates, highly monodisperse capsules containing a broad range of metals were obtained after template removal (Figure 1c). The coordination between TA and metals was confirmed by UV/Vis absorption spectrophotometry, Fourier transform infrared spectrophotometry (FT-IR) and X-ray photoelectron spectroscopy (XPS). UV/Vis spectra of MPN capsule suspensions show new absorbance peaks after metal chelation, which suggests coordination between TA and the respective metals (Figure S2). FT-IR spectra of the Fe^{III}-TA MPN capsules (air-dried) also indicate that the phenolic groups coordinated with metal ions, as evidenced by the reduced intensity of the HO–C stretching peak when compared with non-coordinated TA (Figure S3). Furthermore, the XPS survey scan spectra confirmed the presence of metal in the capsule shells (Figure S4). TA showed a major peak at 533.5 eV and a relatively small peak at 529.4 eV, which can be ascribed to the C=O and HO–C groups, respectively.[14] After chelation with metal ions, the peak of the HO–C group in the O_{1s} spectra shifted from 529.4 eV to a higher binding energy of 531.8 eV (Figure S5, Cu^{II}-TA capsules), which suggests electron transfer from TA to the metals.[15] The MPN films (Cu^{II}-TA) are amorphous materials, as confirmed by X-ray diffraction data (Figure S6).[16]

The morphology of the capsules was characterized by differential interference contrast (DIC) microscopy, scanning electron microscopy (SEM), transmission electron microscopy (TEM), and atomic force microscopy (AFM) (Figure 2, Figures S7 and S8). The MPN capsules were monodisperse and spherical, as observed by DIC microscopy and freeze-dried SEM (Figure 2a, inset). SEM, TEM, and AFM showed collapsed capsules, with folds and creases similar to air-dried polymeric hollow capsules.[17] No excess coordination cluster aggregates were observed on the surface of the MPN capsules in TEM (Figure 2b) or AFM (Figure 2c). Energy-dispersive X-ray (EDX) mapping analysis of MPN capsules demonstrated that the metal distribution patterns matched well with high-angle annular dark-field images (HAADF) and the distribution patterns of C and O maps (Figure 2d). This confirms that the metals were associated with TA and well distributed in the MPN films. AFM was used to probe the material differences between MPN capsules prepared from metals of different oxidation numbers: Cu^{II}-TA, Al^{III}-TA, and Zr^{IV}-TA (Figure S9). The thickness and stability of the MPN films are dependent on the choice of metal and the metal feed concentration (hereafter denoted [M]). Notably, comparison of film thicknesses among these three MPN capsules showed that Zr^{IV}-TA capsules were the thickest and Cu^{II}-TA capsules the thinnest. The film thickness of Cu^{II}-TA capsules increased from 9.0 ± 0.8 nm to 10.7 ± 1.5 nm when the feed [Cu^{II}] changed from 0.08 ([Cu^{II}]:[TA] = 1:3) to 0.72 mM ([Cu^{II}]:[TA] = 3:1). Similarly, the minimum thickness of Zr^{IV}-TA capsules was 11.9 ± 1.2 nm ([Zr^{IV}]:[TA] = 1:3), and raising the [Zr^{IV}] increased the film thickness to 15.4 ± 2.2 nm

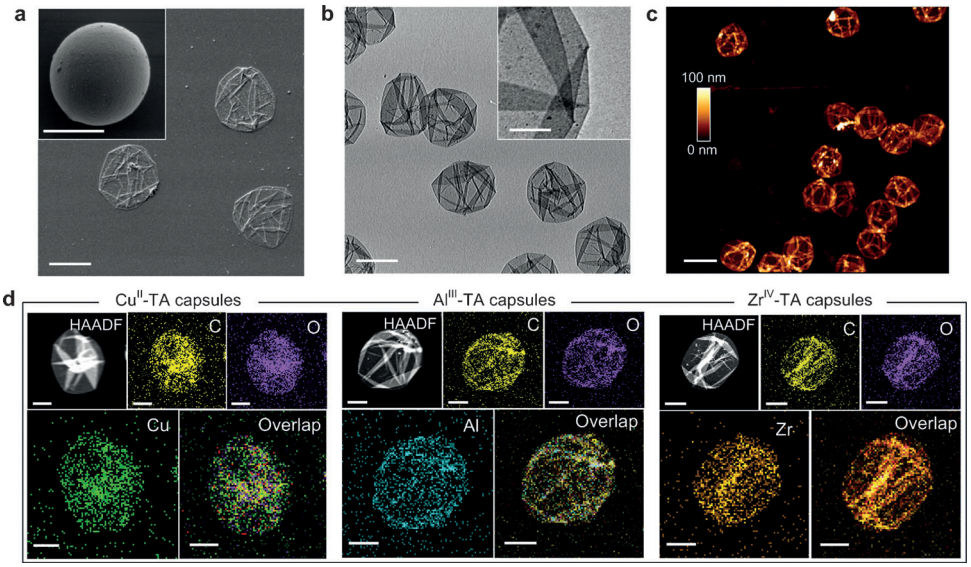

Figure 2. Structural characterization of MPN capsules. a) SEM, b) TEM, and c) AFM images of Cu^{II}-TA capsules. d) EDX elemental mapping of Cu^{II}-TA, Al^{III}-TA and Zr^{IV}-TA capsules. Scale bars are 2 μm in (a–c), 2 μm in the inset of (a), 200 nm in the inset of (b) and 1 μm in (d).

([Zr^{IV}]:[TA] = 3:1). The film thicknesses of Al^{III}-TA films, which increased from 9.9 ± 1.3 nm to 13.6 ± 1.3 nm, showed a similar trend to Cu^{II}-TA and Zr^{IV}-TA. We note that below a [M] of 0.08 mM, capsules for all three metals were difficult to form, while above 0.72 mM the capsules aggregated.

The pH-disassembly kinetics of the MPN capsules prepared from each of the three model metals (Cu^{II}, Al^{III}, Zr^{IV}) were examined. (A moderate [M] of 0.24 mM ([M]:[TA] = 1:1) was used to prepare these capsules.) The stability of the MPN capsules decreased as the pH decreased from 7.4 to 5.0 (Figure 3a). At pH 5.0, over 25% of the Cu^{II}-TA capsules (9.7 ± 1.0 nm) disassembled within 1 h, whereas it took roughly 6 h for 25% of the Al^{III}-TA capsules (10.8 ± 1.3 nm) to disassemble, and even after 168 h, less than 25% of the Zr^{IV}-TA capsules (14.2 ± 1.5 nm) had disassembled. The intermediate disassembly kinetics for the Al^{III}-TA capsules correspond to a desirable profile for drug delivery, as the capsules are relatively stable at the pH of the bloodstream (7.4) and gradually disassemble at lower pH values that correspond to those in endosomal and lysosomal compartments (5.0–6.0). The cytotoxicity of the Al^{III}-TA capsules was determined to be negligible (Figure S10), hence the drug delivery properties of the Al^{III}-TA capsules were investigated with model cargo (dextran-fluorescein isothiocyanate, FITC-dextran). These capsules were incubated with JAWS II cells for different times. The cellular membranes were stained with AlexaFluor (AF) 594-wheat germ agglutinin, and internalization of these capsules was verified by deconvolution fluorescence microscopy (Figure 3b). At the time interval of 16 h, most internalized Al^{III}-TA capsules were intact, retaining their original spherical shape (see yellow arrows in Figure 3b). With increasing incubation time (to 24 h), a larger number of deformed and disassembled Al^{III}-TA capsules were observed (see white arrows in Figure 3b). The intracellular disassembly of Al^{III}-TA capsules provides the potential for tailored drug release, which is of importance for advanced drug delivery.[18]

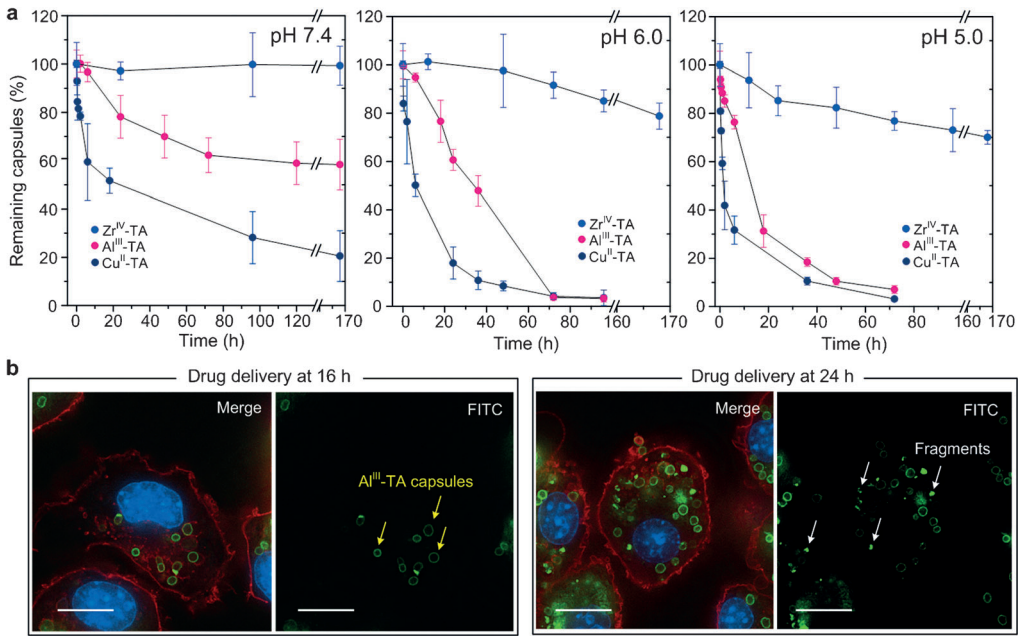

Figure 3. Controlled disassembly of MPN capsules. a) pH-dependent disassembly kinetics of Cu^{II}-TA, Al^{III}-TA and Zr^{IV}-TA capsules at different pH values, as assessed by flow cytometry. The data are mean values ± standard deviation (SD; $N = 3$). b) Degradation of FITC-dextran-loaded Al^{III}-TA capsules in JAWS II cells at different times, as imaged by deconvolution fluorescence microscopy. Green corresponds to FITC-dextran, red to the cell membrane staining, and blue to nuclear staining. The scale bars are 10 μm.

To impart imaging properties to the MPN capsules, we employed 2-thenoyltrifluoroacetone (TTA) and acetylacetone (AA) as coligands to enhance the fluorescence intensities of Eu^{III}-TA and Tb^{III}-TA capsules, respectively, and to demonstrate that guest functional ligands can be easily incorporated into MPN films. Figure 4a shows the fluorescence spectra of these capsules. The red fluorescence observed in the Eu^{III}-TTA-TA capsules is mainly attributed to the $^5D_0 \rightarrow {}^7F_2$ transition around 613 nm[19] and the green fluorescence of the Tb^{III}-AA-TA capsules is ascribed to the $^5D_4 \rightarrow {}^7F_5$ transition around 545 nm.[20] The fluorescence intensity of the Eu^{III}-TTA-TA capsules is dependent on the [Eu^{III}], with an increase in fluorescence intensity dependent on the [Eu^{III}] (Figure S11). The insets of Figure 4a show photographs of the Tb^{III}-AA-TA and Eu^{III}-TTA-TA capsule suspensions (upper) and polydimethylsiloxane (PDMS) coated with a Eu^{III}-TTA-TA film excited at 365 nm (lower).

We extended the investigation of MPN capsules for biomedical imaging by incorporating metals useful for positron emission tomography (PET) and magnetic resonance imaging (MRI). Radioactive $^{64}Cu^{II}$-TA capsules were prepared by adding 5 MBq of ^{64}Cu during MPN film assembly. Figure 4b shows the corresponding PET phantom image, which suggests that the $^{64}Cu^{II}$-TA capsules are efficient PET-active vehicles, and useful for tracking the biodistribution of both loaded drugs and the carrier itself. Therefore, $^{64}Cu^{II}$-TA capsules were injected into healthy BALB/c mice. PET/computed tomography (CT) scans were acquired and the biodistribution of the capsules was evaluated after 30 min. The PET/CT images showed major uptake of the capsules in the liver and minor uptake in the spleen (Figure 4c), which was further confirmed by the post-mortem biodistribution data (Figure S12). This gamma-counter data set revealed general tissue distribution and demonstrated that the $^{64}Cu^{II}$-TA capsules mainly accumulated in the liver and spleen, as a consequence of the reticuloendothelial system that processes microparticles.[7i] It is plausible that the biodistribution of $^{64}Cu^{II}$-TA capsules can be tailored by controlling capsule properties (e.g., size, shape, and surface chemistry) given the versatility of MPN materials.[10b] We then explored the possibility of generating MRI contrast agents by the coordination of Fe^{III}, Mn^{II}, and Gd^{III} into MPN capsules. We performed MR relaxometry experiments with these capsules and determined their relaxivities on a 9.4 T animal MRI system (Figure 4d,e and Figure S13). Among all three samples the Mn^{II}-TA capsules displayed the highest relaxivity r_2, which is of the order of 60 $s^{-1}mM^{-1}$ and generally sufficient for in vivo use.[21]

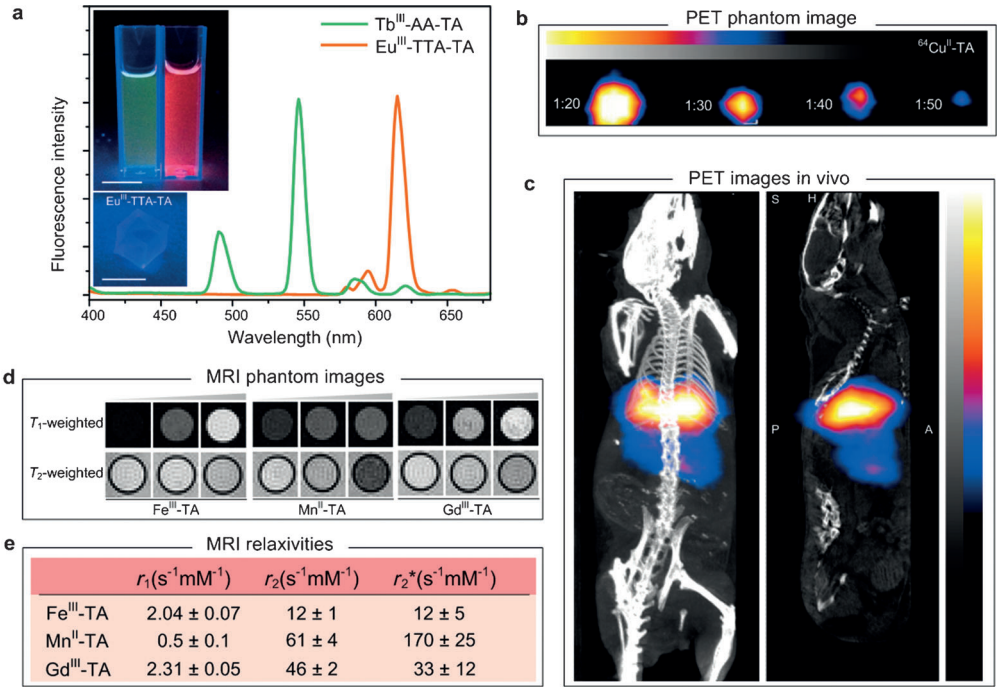

	r_1($s^{-1}mM^{-1}$)	r_2($s^{-1}mM^{-1}$)	r_2*($s^{-1}mM^{-1}$)
Fe^{III}-TA	2.04 ± 0.07	12 ± 1	12 ± 5
Mn^{II}-TA	0.5 ± 0.1	61 ± 4	170 ± 25
Gd^{III}-TA	2.31 ± 0.05	46 ± 2	33 ± 12

Figure 4. Engineering multifunctional MPN capsules for imaging. a) Normalized fluorescence spectra of capsule suspensions of Eu^{III}-TTA-TA and Tb^{III}-AA-TA excited at 360 nm. Insets are photographs of the corresponding capsule suspensions (top), excited at 254 and 365 nm, and of PDMS coated with Eu^{III}-TTA-TA (bottom) excited at 365 nm. Scale bars are 1 cm. b) Pseudo-color PET phantom of suspensions of $^{64}Cu^{II}$-TA capsules at different dilution ratios (stock suspension concentration is 3.2×10^8 capsules per millilitre with an activity of 1 MBq). c) Small-animal PET/CT image of an in vivo model 30 min after injection of 1 MBq $^{64}Cu^{II}$-TA capsules (maximum intensity projection (right), sagittal view (left)). The color scale for all PET image data shows radiotracer uptake with white corresponding to the highest activity and blue to the lowest activity. d) MRI phantom images of capsules immobilized in agarose. Shown are T_1-weighted inversion recovery images (with inversion time $T_I = 1375$ ms) and T_2-weighted spin echo images (with echo time $T_E = 50$ ms) of samples with three different metal concentrations from left to right: 0.02, 0.1, and 0.3 mM (0.15 mM for Gd^{III}-TA). e) Table of MRI relaxivities for Fe^{III}-TA, Mn^{II}-TA, and Gd^{III}-TA capsule suspensions measured with a 9.4 T animal MRI system.

We additionally examined the hybrid, dual-metal capsules for improved functionality as biomedical imaging agents. To test dual-metal incorporation, we assembled (Cu^{II}/Eu^{III}-TTA)-TA capsules that displayed highly distributed signals from Cu and Eu by EDX mapping analysis (Figure 5a). To verify the multimodal capability of MPN capsules, ($^{64}Cu^{II}$/Eu^{III}-TTA)-TA capsules were used for both PET and fluorescence imaging. Figure 5b shows the fluorescence and reconstructed PET/CT images of an aqueous suspension of ($^{64}Cu^{II}$/Eu^{III}-TTA)-TA capsules. Furthermore, multicolor fluorescent MPN capsules were achieved by incorporating Eu^{III}

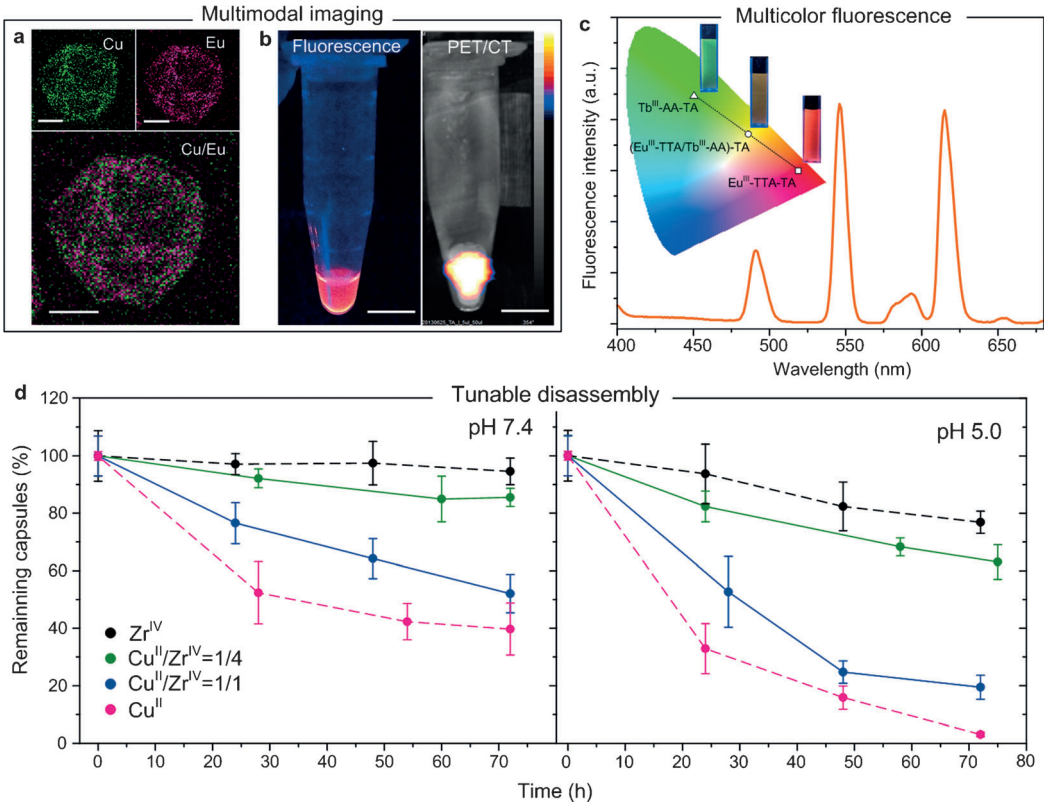

Figure 5. Hybrid dual metal MPN capsules for multimodal imaging, multicolor properties, and tunable disassembly. a) EDX elemental mapping of dual metal (Cu^{II}/Eu^{III}-TTA)-TA capsules. The scale bar is 1 μm. b) Fluorescence (left) and PET/CT pseudo-color (right) images of a suspension of ($^{64}Cu^{II}$/Eu^{III}-TTA)-TA capsules. The scale bars are 1 cm. c) Normalized fluorescence spectra for (Eu^{III}-TTA/Tb^{III}-AA)-TA capsule suspensions excited at 312 nm. The insets are fluorescence images of Eu^{III}-TTA-TA, Tb^{III}-AA-TA, and (Eu^{III}-TTA/Tb^{III}-AA)-TA capsule suspensions and the corresponding locations on the CIE 1931 chromaticity diagram. d) pH-dependent disassembly kinetics of Cu^{II}-TA, Zr^{IV}-TA and hybrid Cu^{II}/Zr^{IV}-TA capsules at different pH, as assessed by flow cytometry. The data are mean values ± SD ($N = 3$).

and Tb^{III} simultaneously (Figure 5c). The strong yellow fluorescence of the (Eu^{III}-TTA/Tb^{III}-AA)-TA capsules corresponds to the expected color in the CIE 1931 chromaticity diagram (inset of Figure 5c). The multicolor fluorescent properties of the MPN films might be of interest in flexible full-color displays, next-generation lighting sources, and bioimaging agents necessary for deciphering multiple biological events simultaneously.[22] Additionally, the degradation profile of the MPN capsules could be tuned by incorporating two metals with different degradation kinetics (Figure 5d). By varying the ratio of Cu^{II}:Zr^{IV}, the kinetics of disassembly at different pH values can be tuned between the disassembly profiles of the single metal MPN capsules.

The wide variety of metals used to demonstrate MPN capsule formation is not only limited to metals useful for biomedical application. Therefore, we demonstrated the catalytic function of Rh^{III}-TA capsules for the hydrogenation of quinoline versus a commercial catalyst, $RhCl(CO)(TPPTS)_2$ (TPPTS = triphenylphosphine-trisulfonated).[23] The initial hydrogenation activities (turnover of frequency, TOF) of both Rh^{III}-TA capsules and $RhCl(CO)(TPPTS)_2$ are quite low when the reaction temperature is below 50 °C (Figure S14). However, a dramatic increase in hydrogenation activity can be observed in Rh^{III}-TA capsules when the reaction temperature changes from 50 to 70 °C; 16 to 103 mol $mol^{-1}\,h^{-1}$, respectively. The catalytic activity of Rh^{III}-TA capsules was significantly greater than $RhCl(CO)(TPPTS)_2$ between 50 and 70 °C, where the maximum initial TOF of $RhCl(CO)(TPPTS)_2$ was only 44 mol $mol^{-1}\,h^{-1}$, which is 43 % of the TOF value for the Rh^{III}-TA capsules.

In summary, we introduced a library of MPNs for the engineering of multifunctional capsules. Various metals were coordinated with tannic acid to form thin films on particulate substrates. EDX mapping analysis demonstrated that the metals were incorporated for both single- and dual-metal MPN capsules. The disassembly of MPN capsules was controlled by changing the metal species and feed concentrations. Similarly, varying the feed concentration of the lanthanide metals allowed for control over the fluorescence intensity of the capsules. Biomedical functionalities for drug delivery, PET, and MRI were successfully imparted to the MPN capsules. The PET activity allowed assessment of the biodistribution of MPN capsules in vivo. The transverse relaxivity r_2 of Mn^{II}-TA capsules is, in principle, large enough for in vivo use of the capsules as MRI contrast agents. Finally, it was demonstrated that Rh^{III}-TA capsules had improved catalysis properties compared with a commercial catalyst. The ability to simultaneously incorporate multiple metals should facilitate the development of MPN capsules useful for a range of applications.

Received: December 23, 2013
Published online: April 2, 2014

Keywords: coordination · fluorescence · multifunctional capsules · organic–inorganic hybrid materials · polyphenols

[1] a) C. Sanchez, H. Arribart, M. M. G. Guille, *Nat. Mater.* **2005**, *4*, 277 – 288; b) Z. Tang, N. A. Kotov, S. Magonov, B. Ozturk, *Nat. Mater.* **2003**, *2*, 413 – 418; c) H. Lee, S. M. Dellatore, W. M. Miller, P. B. Messersmith, *Science* **2007**, *318*, 426 – 430; d) E. Munch, M. E. Launey, D. H. Alsem, E. Saiz, A. P. Tomsia, R. O. Ritchie, *Science* **2008**, *322*, 1516 – 1520; e) C. J. Hawker, K. L. Wooley, *Science* **2005**, *309*, 1200 – 1205.

[2] S. Sudo, T. Fujikawa, T. Nagakura, T. Ohkubo, K. Sakaguchi, M. Tanaka, K. Nakashima, T. Takahashi, *Nature* **1997**, *387*, 563 – 564.

[3] D. J. Rubin, A. Miserez, J. H. Waite, *Adv. Insect Physiol.* **2010**, *38*, 75 – 133.

[4] J. Barrett, *Nature* **1967**, *215*, 733 – 735.

[5] J. Alben, P. Moh, F. Fiamingo, R. Altschuld, *Proc. Natl. Acad. Sci. USA* **1981**, *78*, 234 – 237.

[6] J. H. Waite, M. L. Tanzer, *Science* **1981**, *212*, 1038 – 1040.

[7] a) H. Li, M. Eddaoudi, M. O'Keeffe, O. M. Yaghi, *Nature* **1999**, *402*, 276 – 279; b) R. Matsuda, R. Kitaura, S. Kitagawa, Y. Kubota, R. V. Belosludov, T. C. Kobayashi, H. Sakamoto, T. Chiba, M. Takata, Y. Kawazoe, *Nature* **2005**, *436*, 238 – 241; c) M. Oh, C. A. Mirkin, *Nature* **2005**, *438*, 651 – 654; d) S. C. Warren, M. R. Perkins, A. M. Adams, M. Kamperman, A. A. Burns, H. Arora, E. Herz, T. Suteewong, H. Sai, Z. Li, *Nat. Mater.* **2012**, *11*, 460 – 467; e) N. C. Gianneschi, M. S. Masar, C. A. Mirkin, *Acc. Chem. Res.* **2005**, *38*, 825 – 837; f) O. K. Farha, A. Ö. Yazaydın, I. Eryazici, C. D. Malliakas, B. G. Hauser, M. G. Kanatzidis, S. T. Nguyen, R. Q. Snurr, J. T. Hupp, *Nat. Chem.* **2010**, *2*, 944 – 948; g) X. Zhao, B. Xiao, A. J. Fletcher, K. M. Thomas, D. Bradshaw, M. J. Rosseinsky, *Science* **2004**, *306*, 1012 – 1015; h) H. Deng, S. Grunder, K. E. Cordova, C. Valente, H. Furukawa, M. Hmadeh, F. Gándara, A. C. Whalley, Z. Liu, S. Asahina, *Science* **2012**, *336*, 1018 – 1023; i) P. Horcajada, T. Chalati, C. Serre, B. Gillet, C. Sebrie, T. Baati, J. F. Eubank, D. Heurtaux, P. Clayette, C. Kreuz, *Nat. Mater.* **2009**, *9*, 172 – 178; j) L. Hamon, C. Serre, T. Devic, T. Loiseau, F. Millange, G. Férey, G. D. Weireld, *J. Am. Chem. Soc.* **2009**, *131*, 8775 – 8777; k) A. M. Spokoyny, D. Kim, A. Sumrein, C. A. Mirkin, *Chem. Soc. Rev.* **2009**, *38*, 1218 – 1227; l) W. L. Leong, J. J. Vittal, *Chem. Rev.* **2011**, *111*, 688 – 764; m) R. Nishiyabu, C. Aimé, R. Gondo, T. Noguchi, N. Kimizuka, *Angew. Chem.* **2009**, *121*, 9629 – 9632; *Angew. Chem. Int. Ed.* **2009**, *48*, 9465 – 9468; n) B. Hoskins, R. Robson, *J. Am. Chem. Soc.* **1990**, *112*, 1546 – 1554; o) J. D. Rocca, D. Liu, W. Lin, *Acc. Chem. Res.* **2011**, *44*, 957 – 968.

[8] a) G. Liang, J. Xu, X. Wang, *J. Am. Chem. Soc.* **2009**, *131*, 5378 – 5379; b) X. Roy, J. K.-H. Hui, M. Rabnawaz, G. Liu, M. J. MacLachlan, *J. Am. Chem. Soc.* **2011**, *133*, 8420 – 8423.

[9] a) R. Ameloot, F. Vermoortele, W. Vanhove, M. B. Roeffaers, B. F. Sels, D. E. De Vos, *Nat. Chem.* **2011**, *3*, 382 – 387; b) A. Carné-Sánchez, I. Imaz, M. Cano-Sarabia, D. Maspoch, *Nat. Chem.* **2013**, *5*, 203 – 211; c) M. Pang, A. J. Cairns, Y. Liu, Y. Belmabkhout, H. C. Zeng, M. Eddaoudi, *J. Am. Chem. Soc.* **2013**, *135*, 10234 – 10237.

[10] a) J. Shi, L. Zhang, Z. Jiang, *ACS Appl. Mater. Interfaces* **2011**, *3*, 881 – 889; b) H. Ejima, J. J. Richardson, K. Liang, J. P. Best, M. P. van Koeverden, G. K. Such, J. Cui, F. Caruso, *Science* **2013**, *341*, 154 – 157.

[11] X. Wang, Z. Jiang, J. Shi, Y. Liang, C. Zhang, H. Wu, *ACS Appl. Mater. Interfaces* **2012**, *4*, 3476 – 3483.

[12] H. J. Lee, W. Cho, M. Oh, *Chem. Commun.* **2012**, *48*, 221 – 223.

[13] a) R. C. Hider, Z. D. Liu, H. H. Khodr, *Methods Enzymol.* **2001**, *335*, 190 – 203; b) M. Andjelković, J. Van Camp, B. De Meulenaer, G. Depaemelaere, C. Socaciu, M. Verloo, R. Verhe, *Food Chem.* **2006**, *98*, 23 – 31; c) S. Clemens, *Planta* **2001**, *212*, 475 – 486; d) T. S. Sileika, D. G. Barrett, R. Zhang, K. H. A. Lau, P. B. Messersmith, *Angew. Chem.* **2013**, *125*, 10966 – 10970; *Angew. Chem. Int. Ed.* **2013**, *52*, 10766 – 10770.

[14] J. Guo, H. Wu, X. Liao, B. Shi, *J. Phys. Chem. C* **2011**, *115*, 23688 – 23694.

[15] X. Huang, X. Liao, B. Shi, *J. Hazard. Mater.* **2009**, *170*, 1141 – 1148.

[16] G. J. Long, G. Longworth, P. Battle, A. K. Cheetham, R. V. Thundathil, D. Beveridge, *Inorg. Chem.* **1979**, *18*, 624 – 632.

[17] a) M. M. Kamphuis, A. P. Johnston, G. K. Such, H. H. Dam, R. A. Evans, A. M. Scott, E. C. Nice, J. K. Heath, F. Caruso, *J. Am. Chem. Soc.* **2010**, *132*, 15881 – 15883; b) G. K. Such, E. Tjipto, A. Postma, A. P. Johnston, F. Caruso, *Nano Lett.* **2007**, *7*, 1706 – 1710.

[18] Y. Qiu, K. Park, *Adv. Drug Delivery Rev.* **2012**, *64*, 49 – 60.

[19] F. S. Richardson, *Chem. Rev.* **1982**, *82*, 541 – 552.

[20] S. Petit, F. Baril-Robert, G. Pilet, C. Reber, D. Luneau, *Dalton Trans.* **2009**, 6809 – 6815.

[21] Y. Gossuin, P. Gillis, A. Hocq, Q. L. Vuong, A. Roch, *Wiley Interdiscip. Rev. Nanomed. Nanobiotechnol.* **2009**, *1*, 299 – 310.

[22] a) J. E. Kwon, S. Park, S. Y. Park, *J. Am. Chem. Soc.* **2013**, *135*, 11239 – 11246; b) M. Green, P. Williamson, M. Samalova, J. Davis, S. Brovelli, P. Dobson, F. Cacialli, *J. Mater. Chem.* **2009**, *19*, 8341 – 8346.

[23] J. Lee, O. K. Farha, J. Roberts, K. A. Scheidt, S. T. Nguyen, J. T. Hupp, *Chem. Soc. Rev.* **2009**, *38*, 1450 – 1459.

